Electronic Supplementary Material (ESI) for CrystEngComm.

Electronic Supplementary Information

Alkyl-Substituted Bis(4-((9H-fluoren-9-ylidene)methyl)phenyl)thiophenes: Weakening of Intermolecular Interactions and Additive-Assisted Crystallization

Alina A. Sonina, Christina S. Becker, Anatoly D. Kuimov, Inna K. Shundrina, Vladislav Yu. Komarov and Maxim S. Kazantsev

1. Characterization

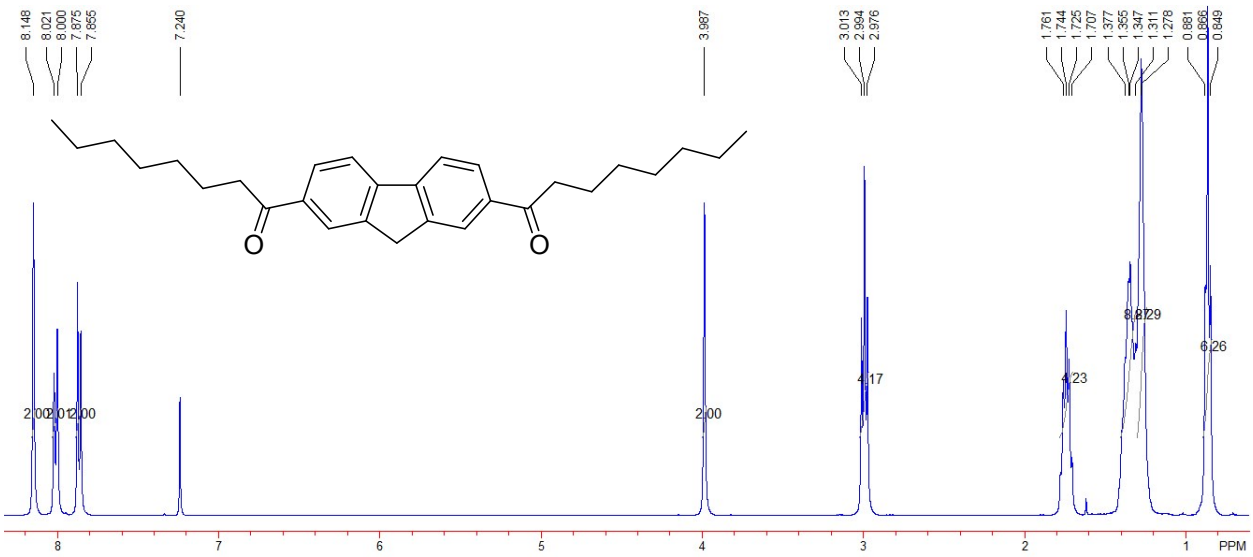

Figure S1. ^{1}H NMR spectrum of compound **1b** in $CDCl_3$.

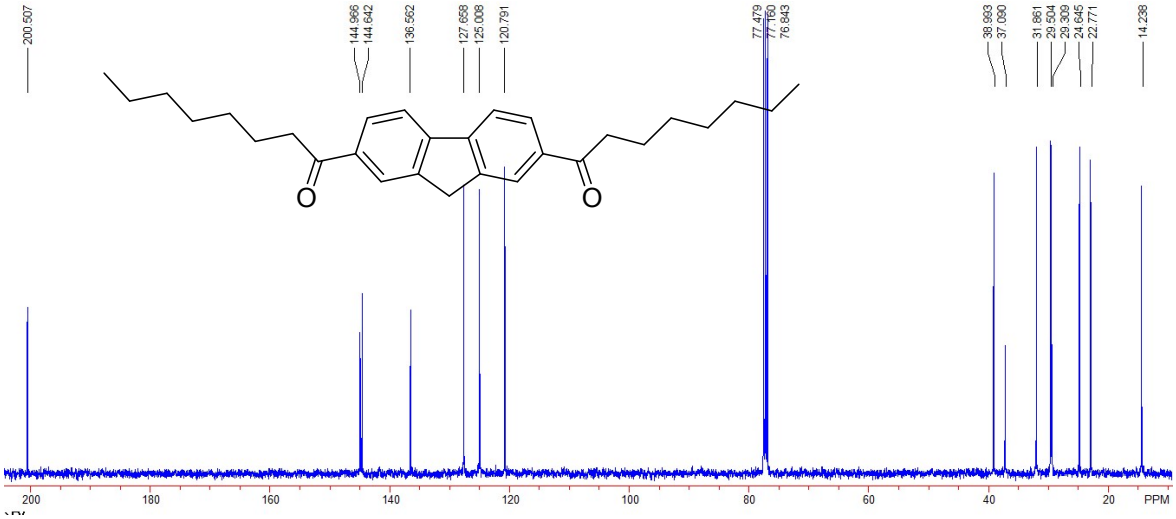

Figure S2. ^{13}C NMR spectrum of compound **1b** in $CDCl_3$.

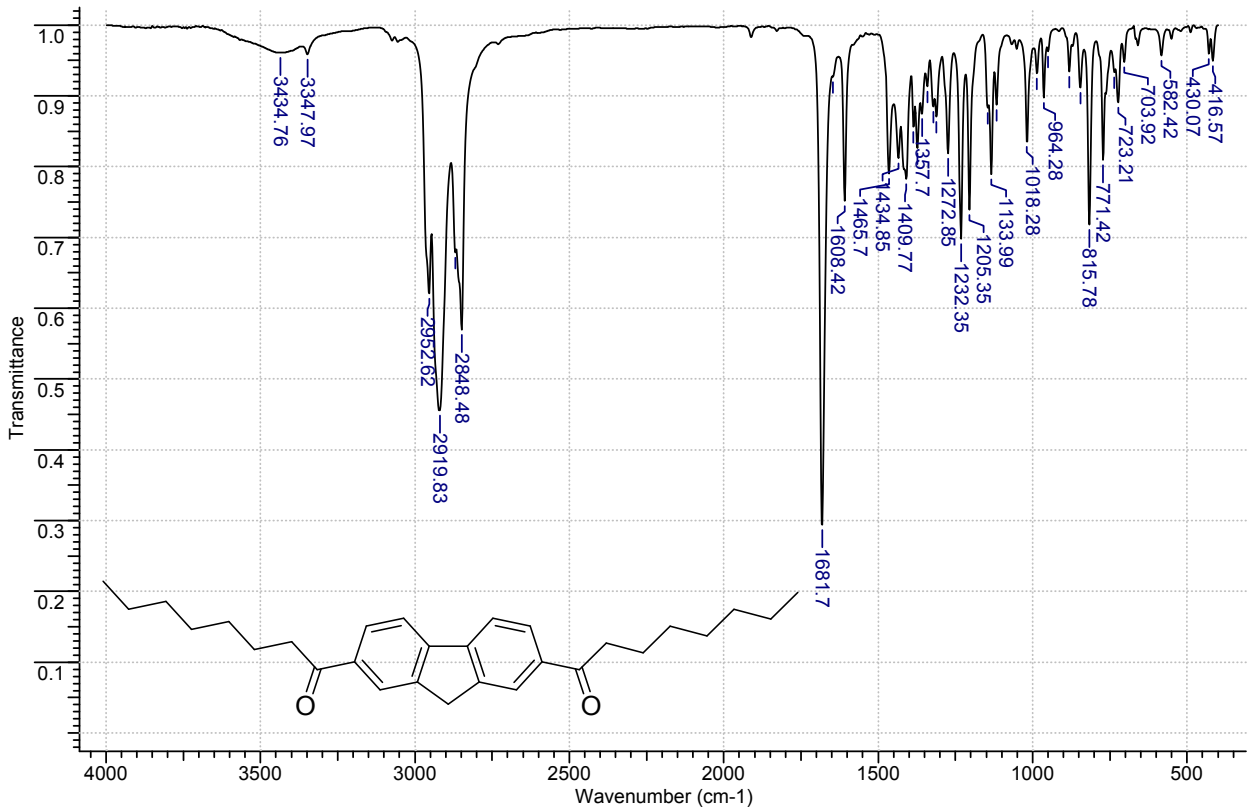

Figure S3. IR spectrum of compound **1b** in KBr pellets.

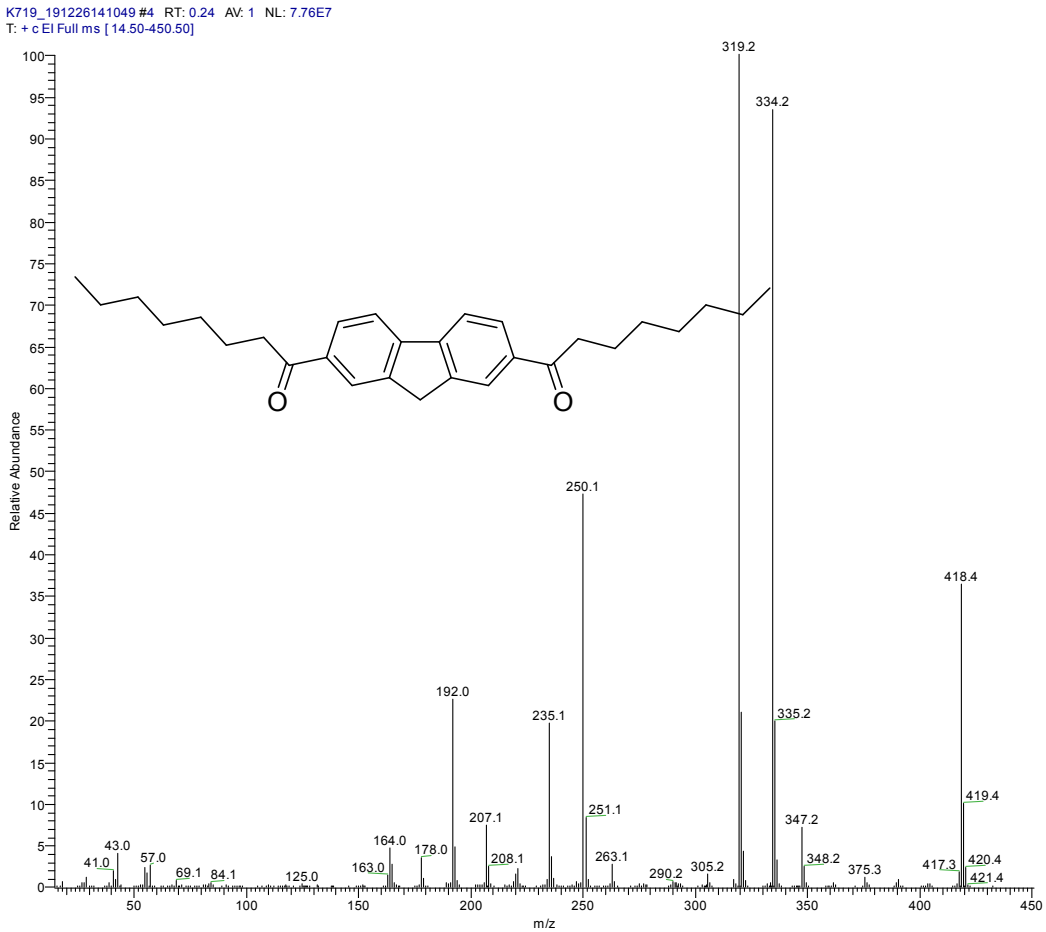

Figure S4. HRMS spectrum of compound **1b** (Tsource=65 ˚C, Tprobe=200 ˚C).

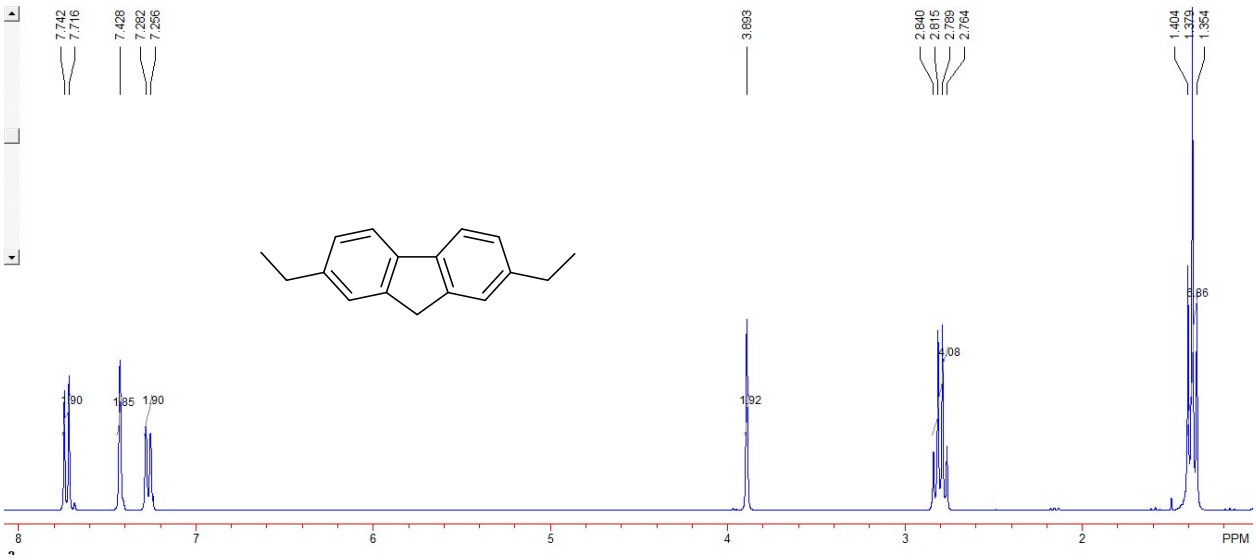

Figure S5. ^{1}H NMR spectrum of compound **2a** in $CDCl_3$.

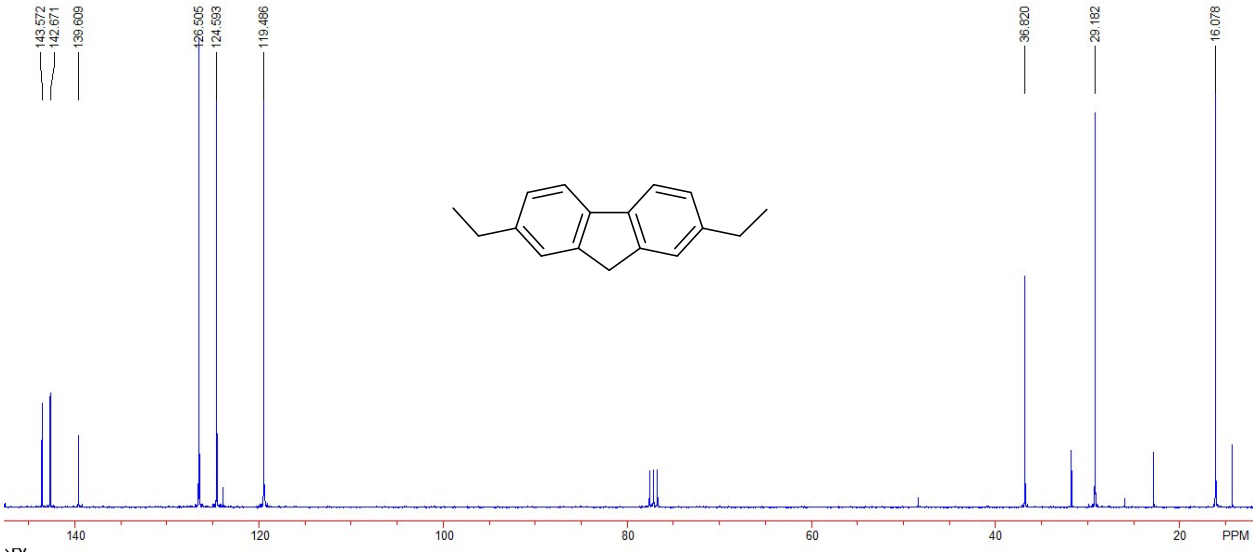

Figure S6. ^{13}C NMR spectrum of compound **2a** in $CDCl_3$.

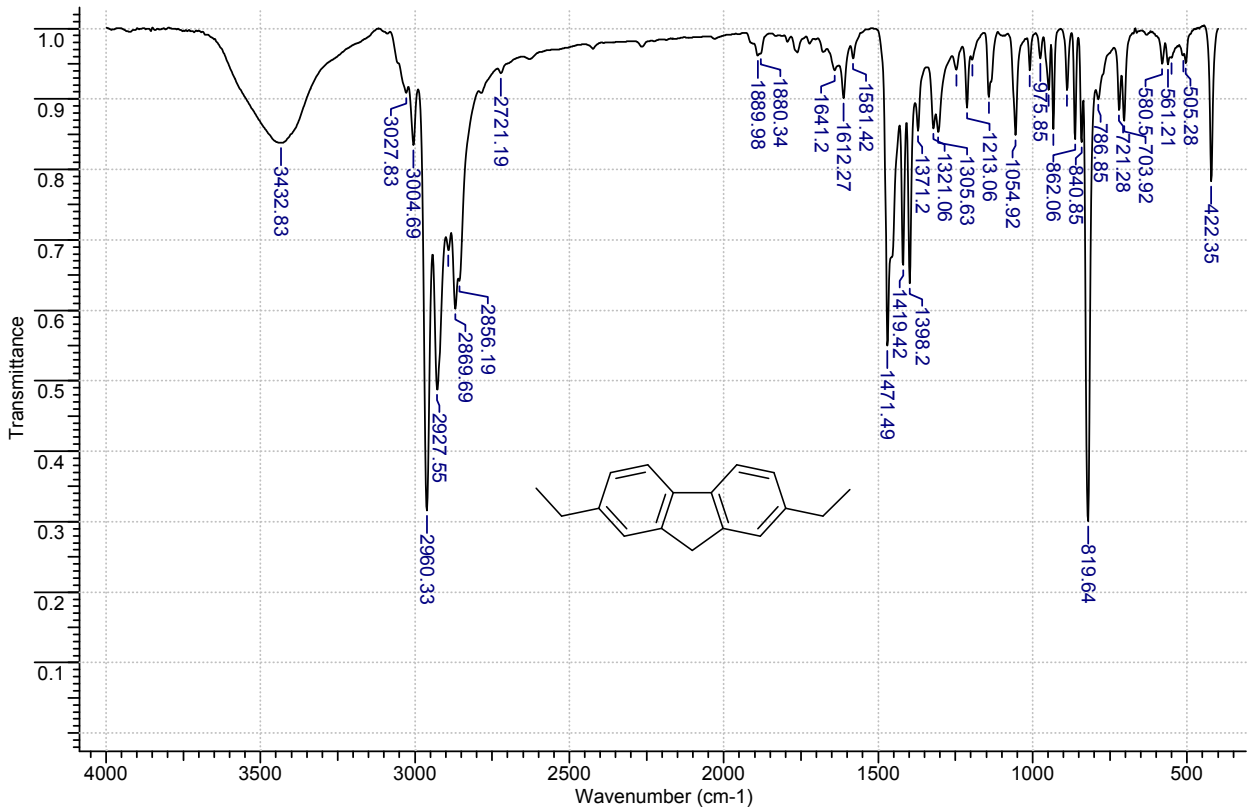

Figure S7. IR spectrum of compound **2a** in KBr pellets.

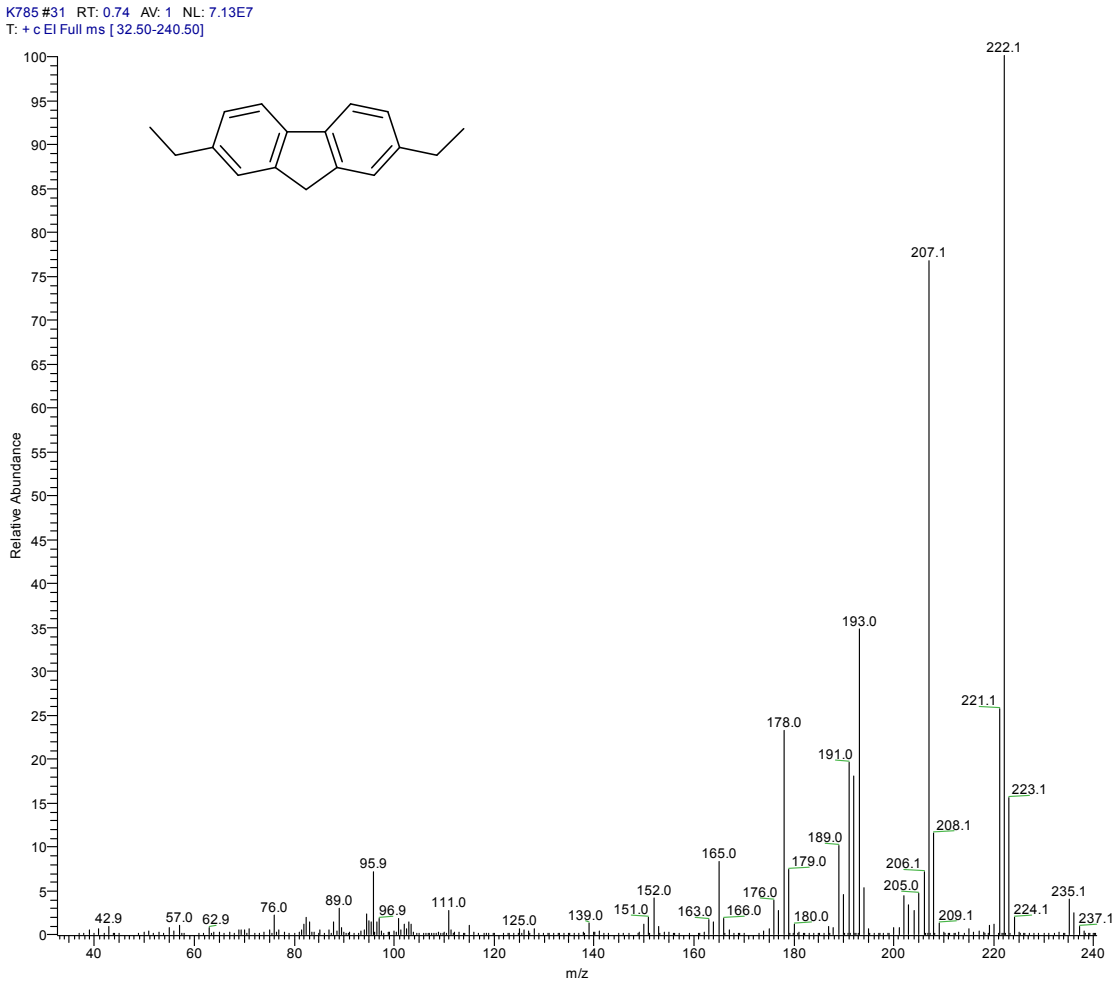

Figure S8. HRMS spectrum of compound **2a** (Tsource=50 ˚C).

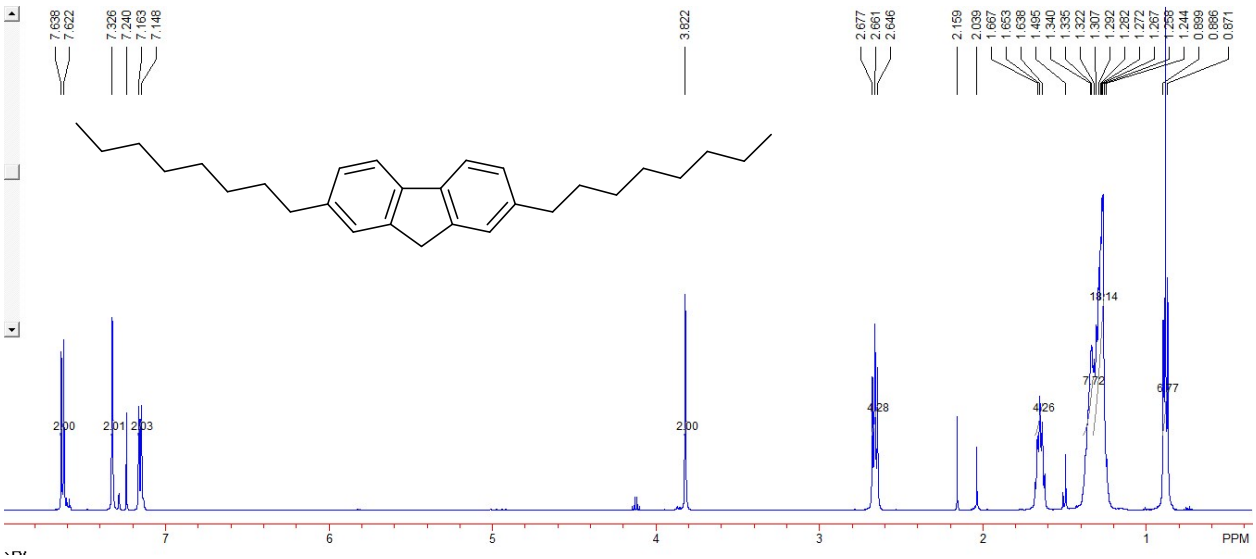

Figure S9. ^{1}H NMR spectrum of compound **2b** in $CDCl_3$.

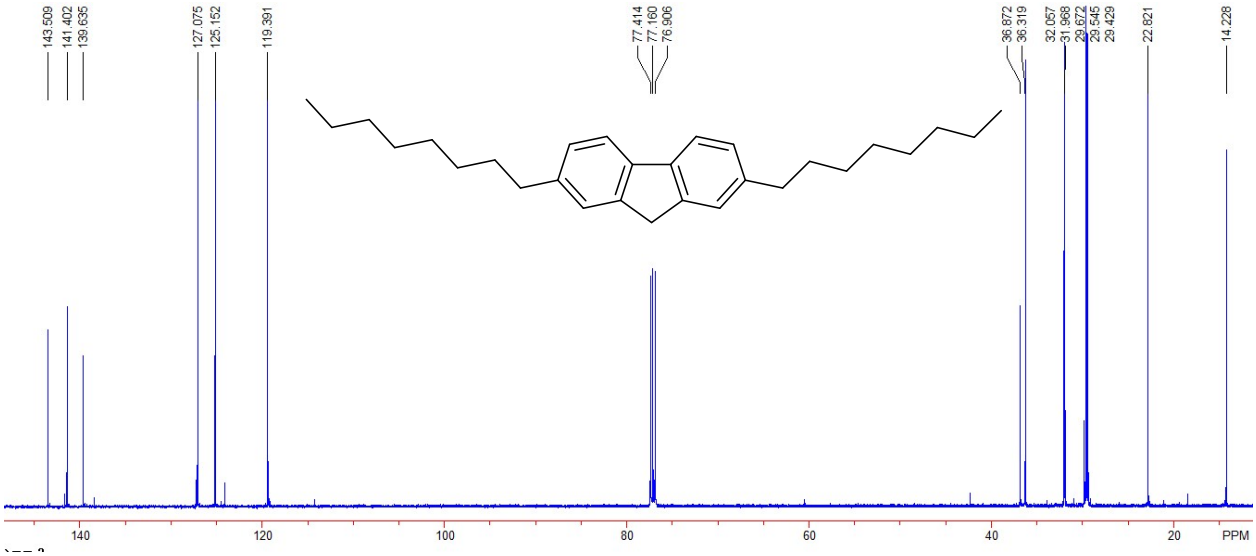

Figure S10. ^{13}C NMR spectrum of compound **2b** in $CDCl_3$.

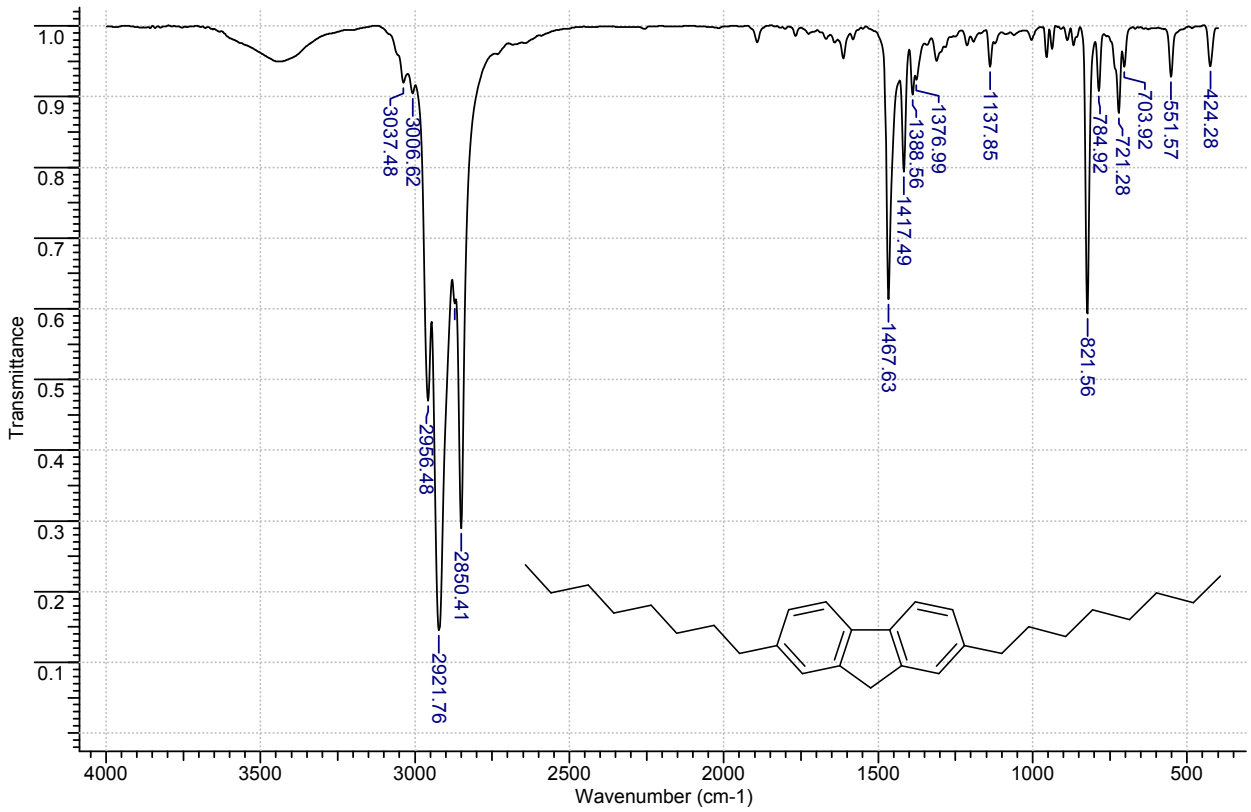

Figure S11. IR spectrum of compound **2b** in KBr pellets.

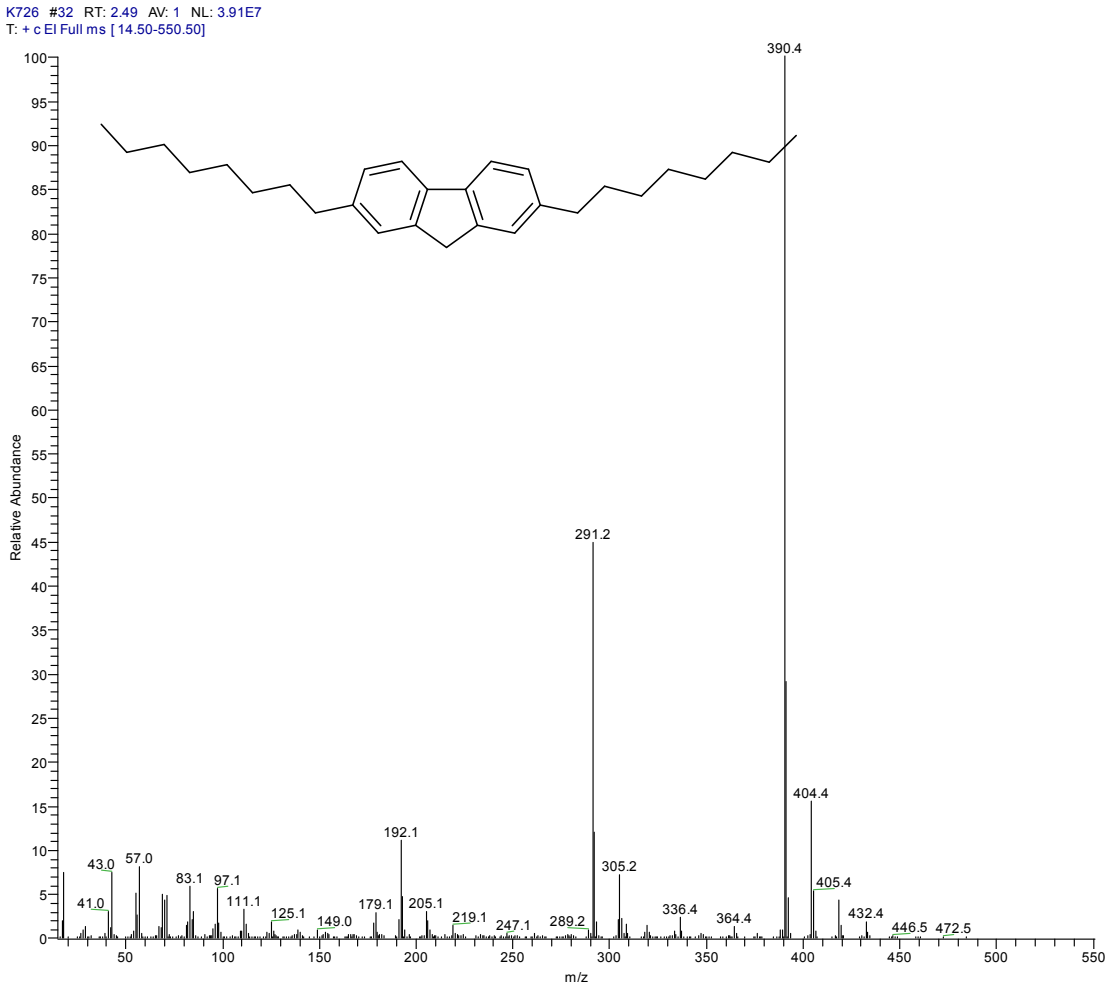

Figure S12. HRMS spectrum of compound **2b** (Tsource=50 ˚C, Tprobe=185 ˚C).

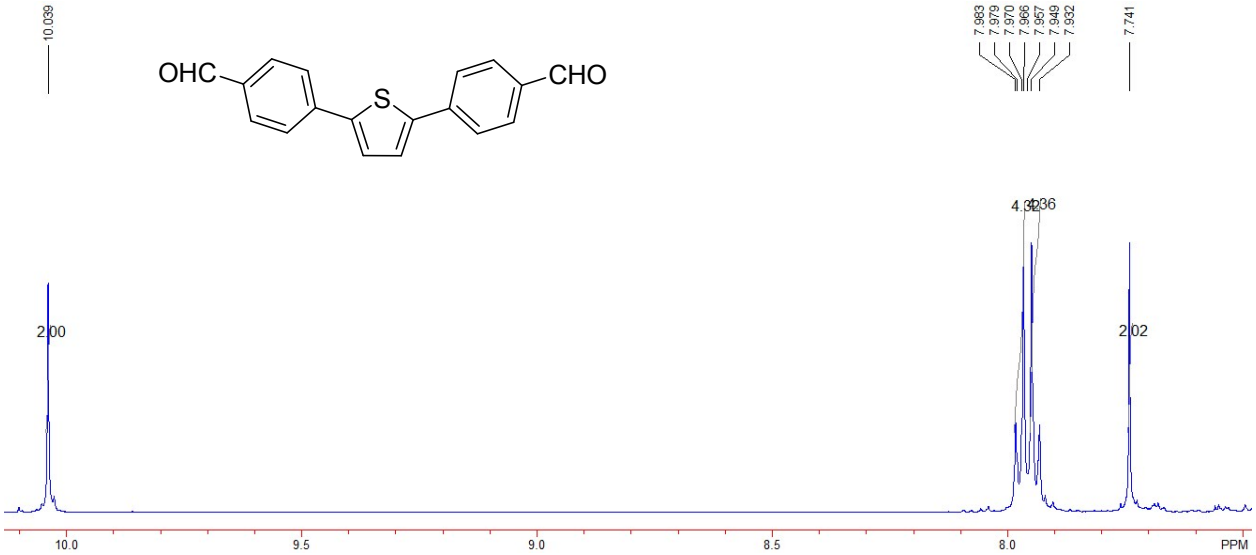

Figure S13. ^{1}H NMR spectrum of compound **3** in $(CD_3)CO$.

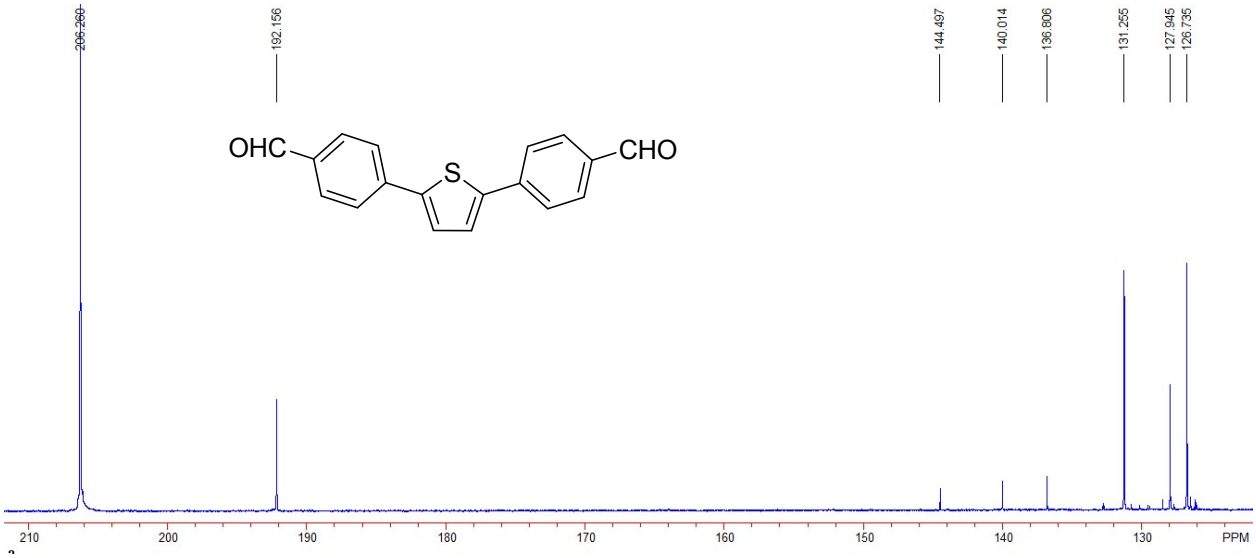

Figure S14. ^{13}C NMR spectrum of compound **3** in $(CD_3)CO$.

Figure S15. ^{1}H NMR spectrum of compound **C2-BFMPT** (+ toluene 1:1) in $CDCl_3$.

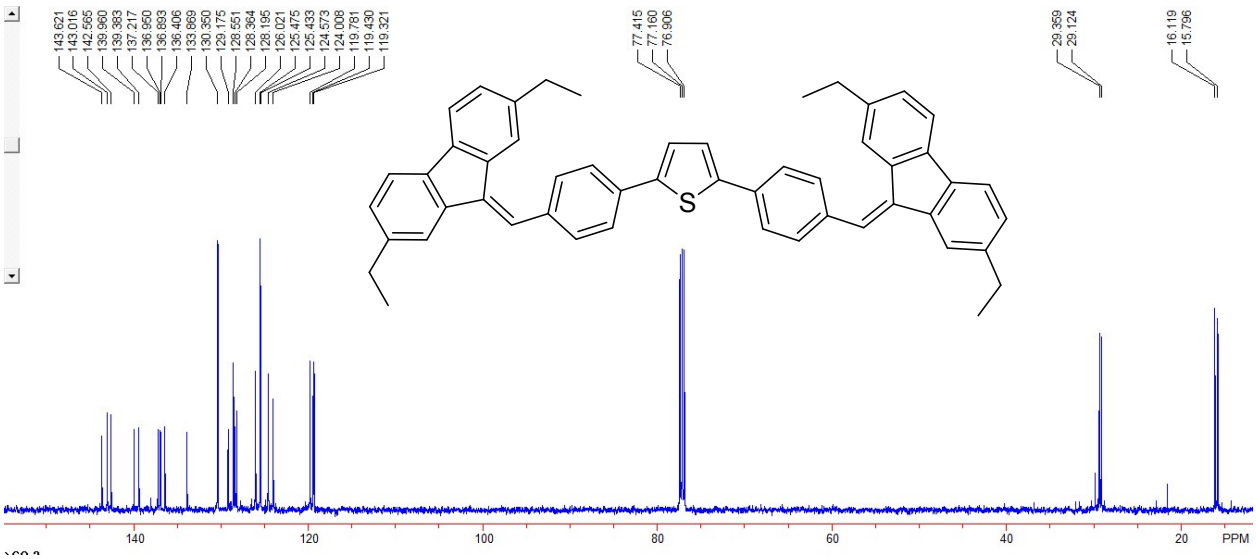

Figure S16. ^{13}C NMR spectrum of compound **C2-BFMPT** in $CDCl_3$.

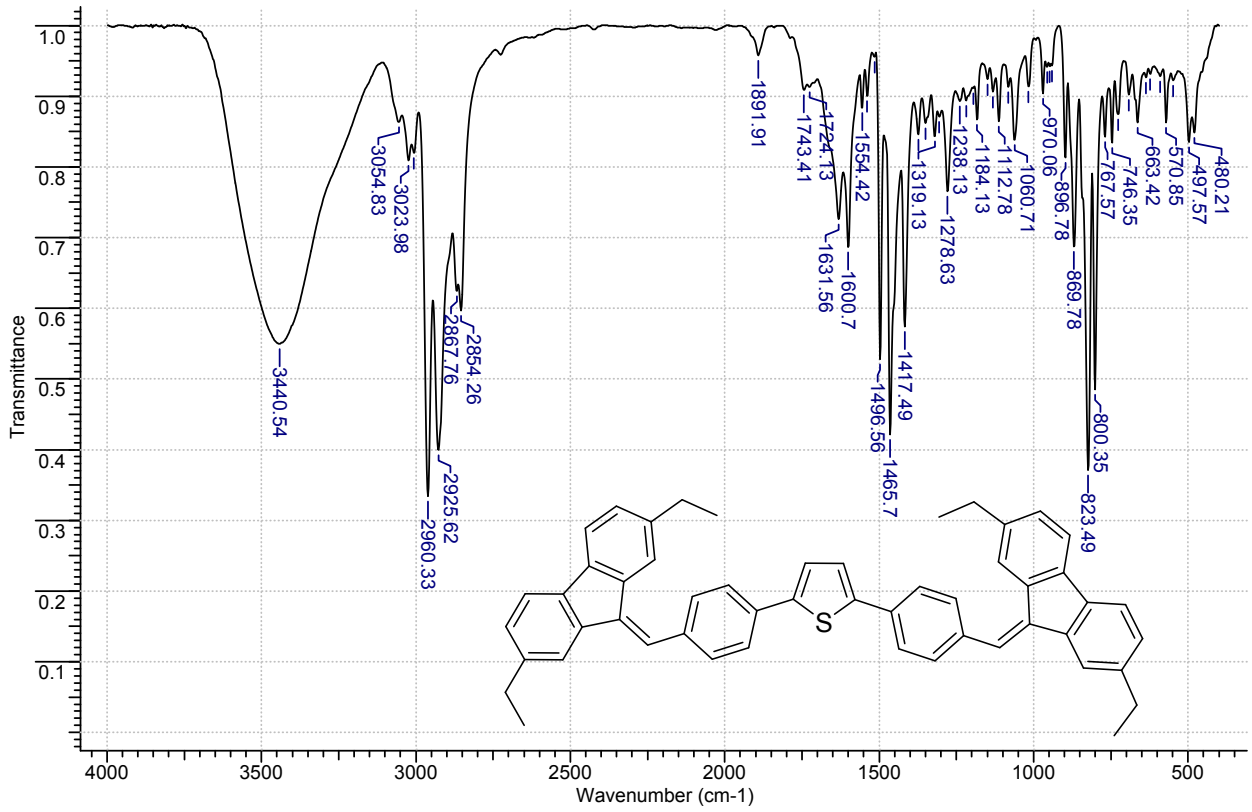

Figure S17. IR spectrum of compound **C2-BFMPT** in KBr pellets.

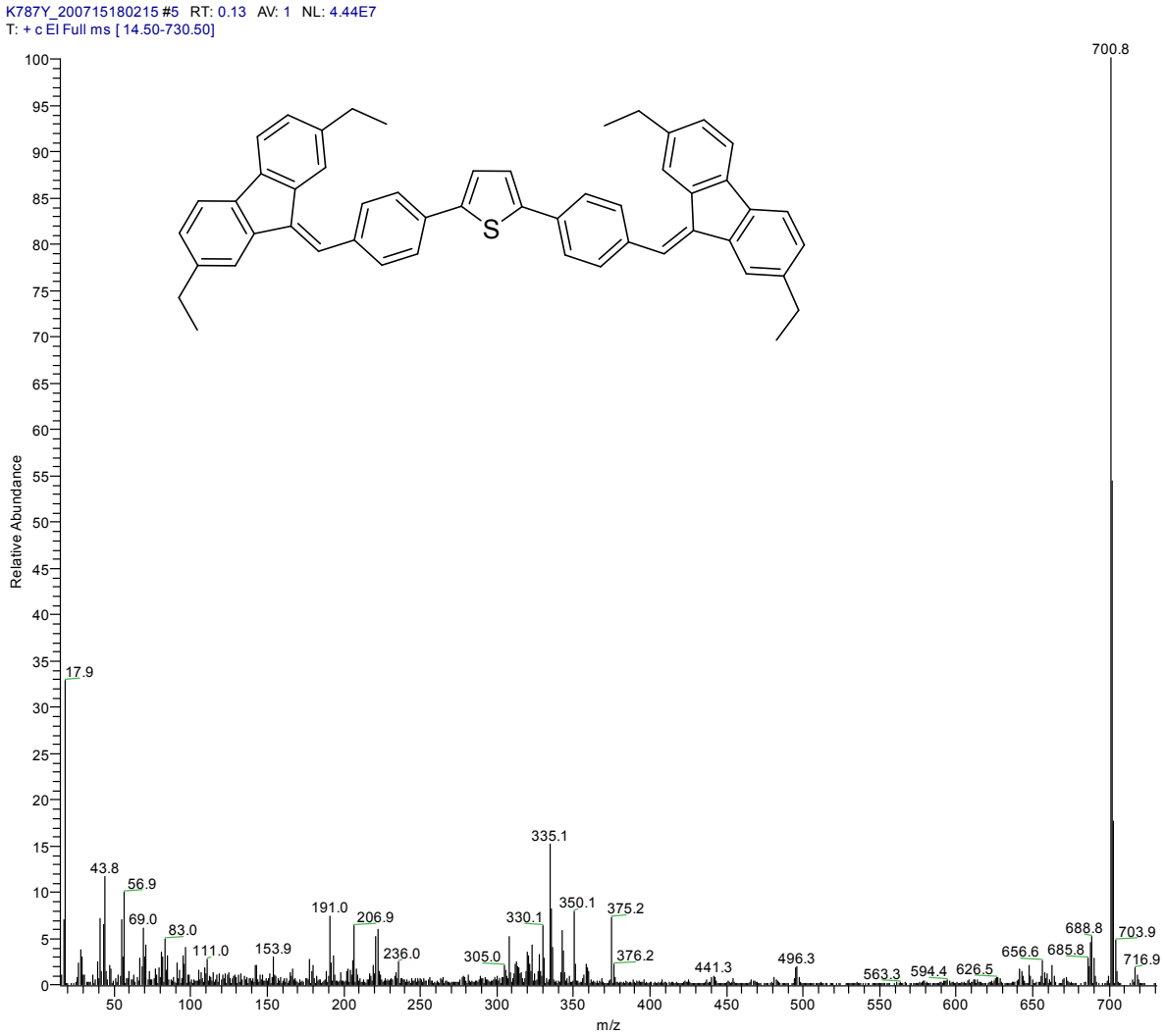

Figure S18. HRMS spectrum of compound **C2-BFMPT** (Tsource=95 ˚C, Tprobe=340 ˚C).

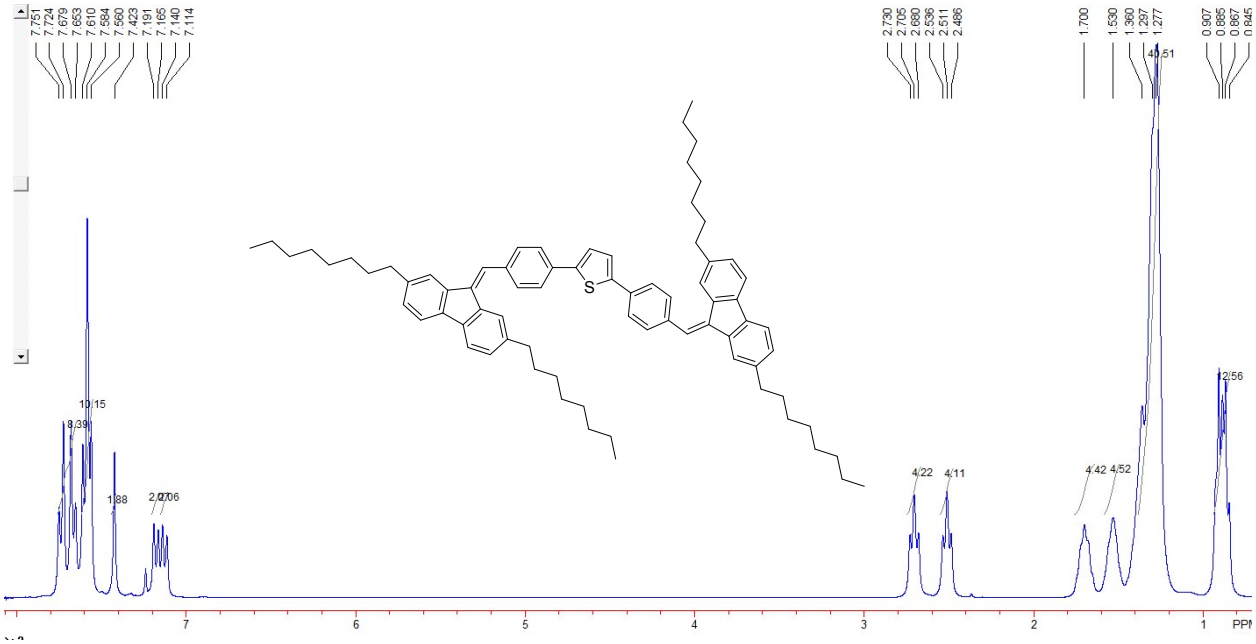

Figure S19. ^{1}H NMR spectrum of compound **C8-BFMPT** in $CDCl_3$.

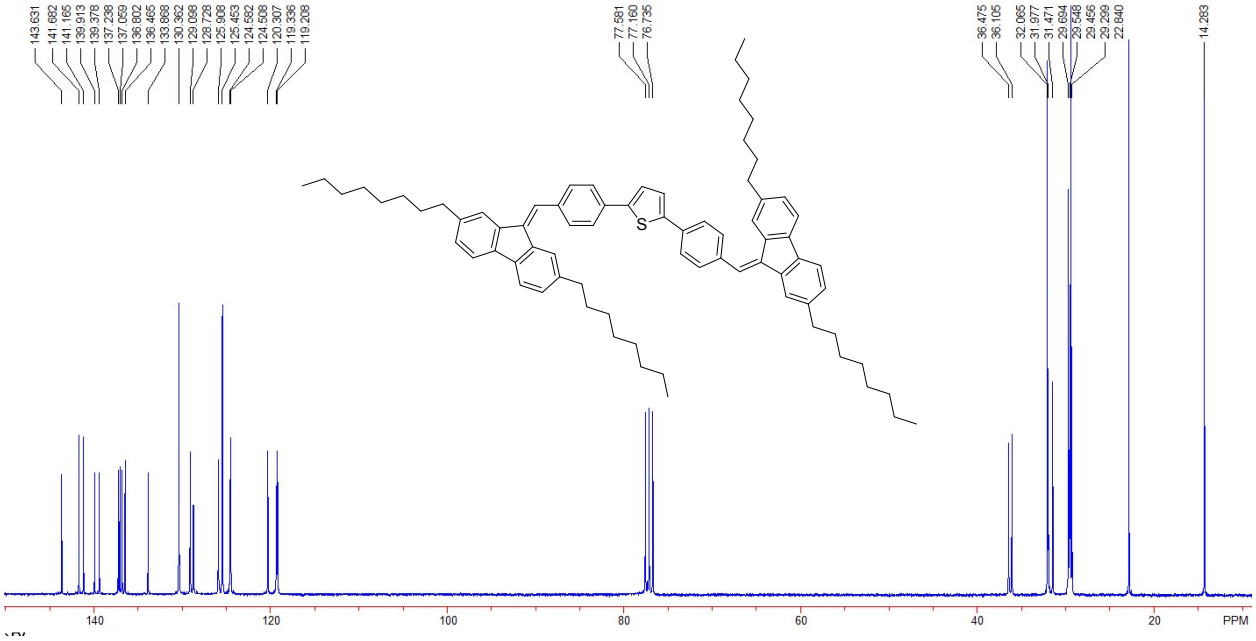

Figure S20. ^{13}C NMR spectrum of compound **C8-BFMPT** in $CDCl_3$.

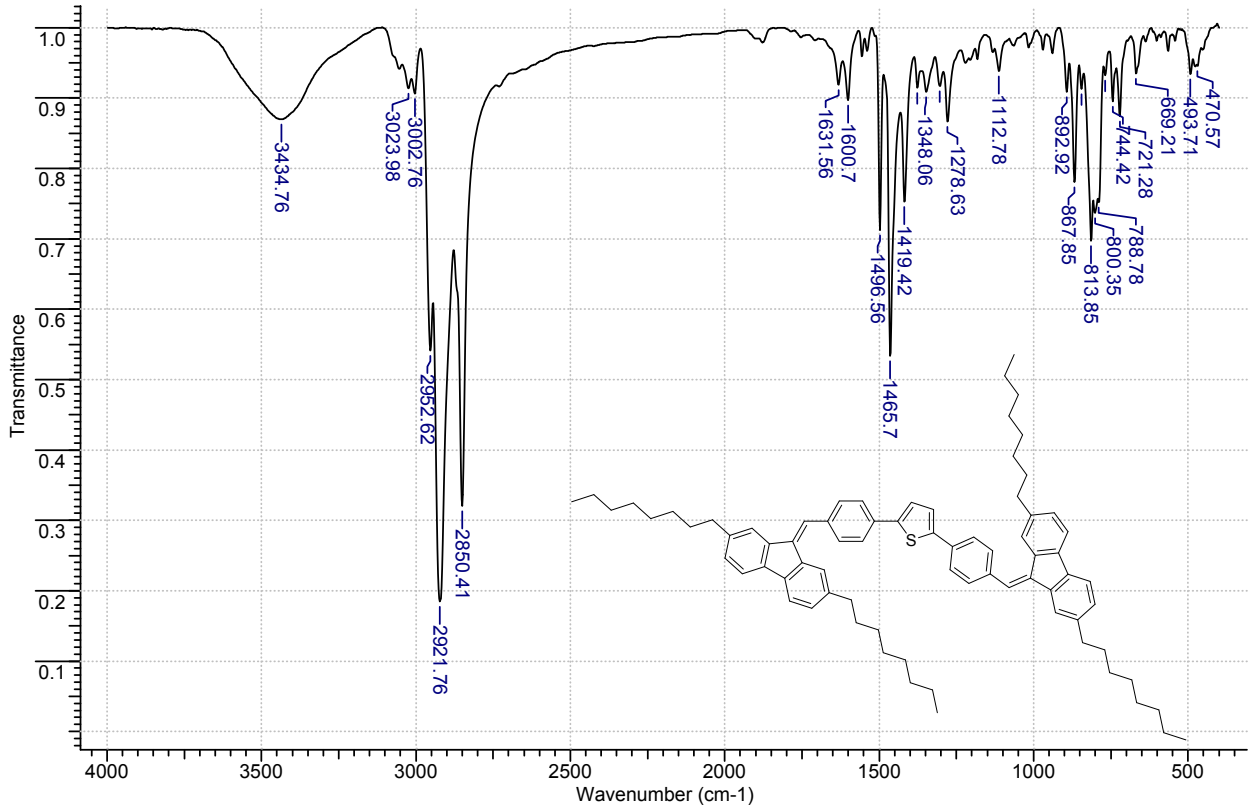

Figure S21. IR spectrum of compound **C8-BFMPT** in KBr pellets.

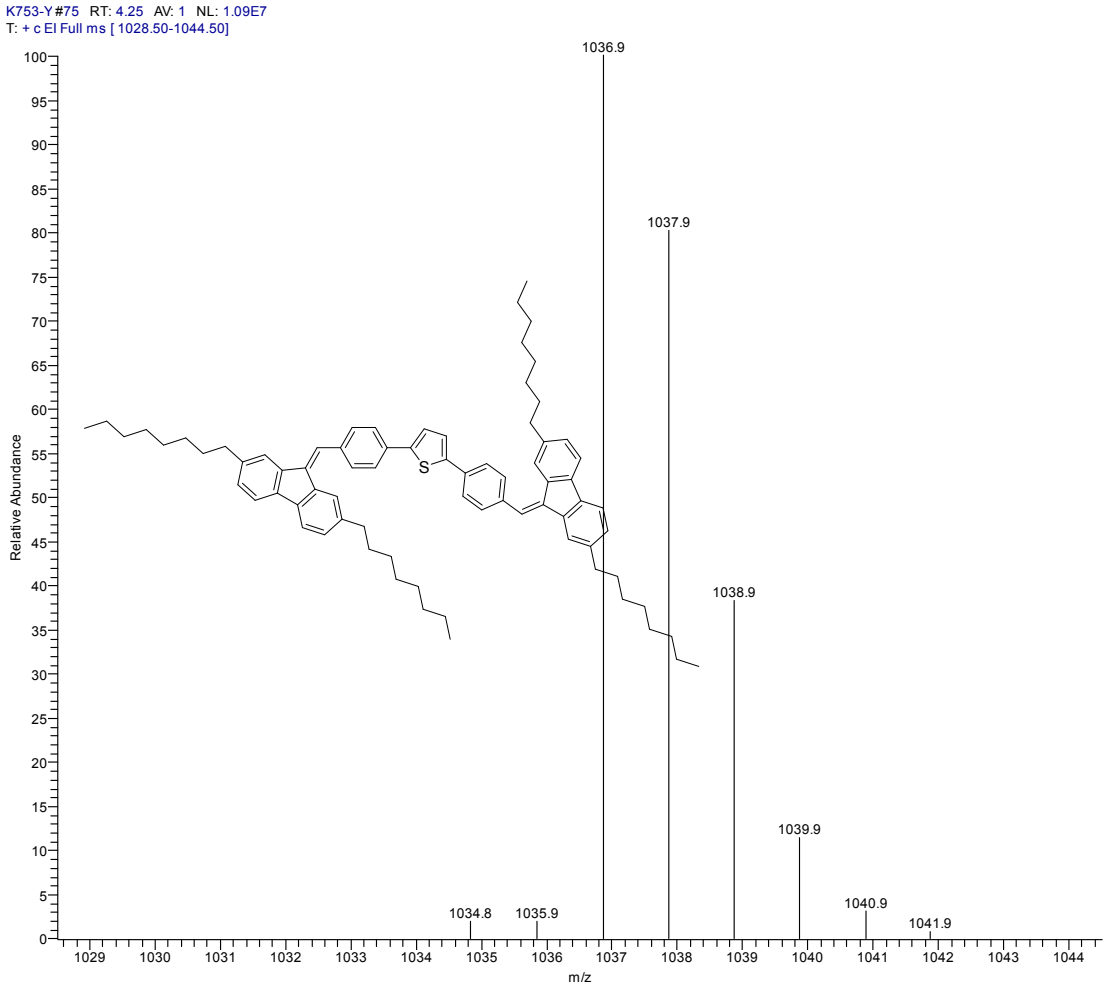

Figure S22. HRMS spectrum of compound **C8-BFMPT** (Tsource=100 ˚C, Tprobe=340 ˚C).

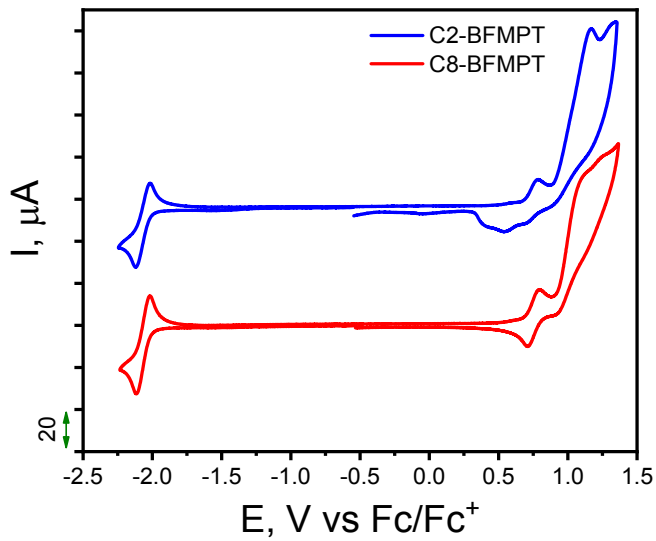

Figure S23. Cyclic voltammograms of C2-BFMPT (blue) and C8-BFMPT (red) in CH_2Cl_2 solution.

2. Crystal data

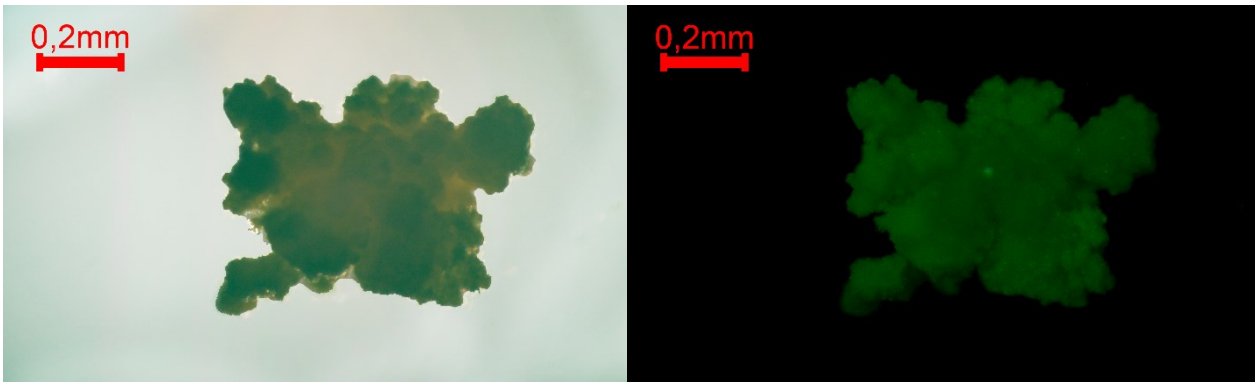

Figure S24. Optical image in transmitted light (left) and under blue laser irradiation (right) of C8-BFMPT polycrystalline sample obtained in neat conditions (form I).

Table S1. Crystallographic, structural data and experimental details for C2-BFMPT and C8-BFMPT Form II at 200K and 80K.

Compound	C2-BFMPT		C8-BFMPT Form II	
Empirical formula	$C_{52}H_{44}S$		$C_{76}H_{92}S$	
Molecular weight	700.93		1037.55	
Crystal system, space group	Monoclinic, $P2_1$		Monoclinic, $P2_1/c$	
Temperature, K	80(2)	200(1)	80(2)	200(1)
Radiation	CuKa	MoKa	CuKa	MoKa
a, *b*, *c* (Å)	16.5329(4) 9.1211(2) 24.9977(6)	16.581 (6), 9.216 (3), 25.101 (9)	5.6172(4), 56.654(4), 19.3396(13)	5.589 (1), 56.50 (1), 19.860 (4)
β (°)	90.6940(10)	90.1 (1)	91.715(2)	91.756 (5)
Volume (Å^3)	3769.33(15)	3836 (2)	6151.8(7)	6268 (2)
Z	4	4	4	4
$D_{calcd.}$ (g·cm^{-3})	1.235	1.214	1.120	1.099
μ (mm^{-1})	1.027	0.12	0.77	0.09
Crystal size (mm)	0.16 × 0.06 × 0.01	1.00 × 0.12 × 0.06	0.14 × 0.04 × 0.02	0.67 × 0.30 × 0.14
No. of measured, independent and observed [$I > 2\sigma(I)$] reflections	41901, 5183, 3898	30271, 8241, 7315	30250, 3766, 2597	25860, 4531, 3157
R_{int}	0.088	0.058	0.049	0.076
Θ range (°)	2.67 – 46.12	2.59 19.55	2.41 38.05	2.32 19.26
Range of h, k, l	$-14 \le h \le 14$, $-7 \le k \le 7$, $-21 \le l \le 21$	$-16 \le h \le 16$, $-9 \le k \le 9$, $-25 \le l \le 25$	$-4 \le h \le 4$, $-47 \le k \le 47$, $-16 \le l \le 16$	$-4 \le h \le 5$, $-50 \le k \le 49$, $-17 \le l \le 17$
$R[F^2 > 2\sigma(F^2)]$, $wR(F^2)$, S	0.071, 0.207, 1.04	0.046, 0.12, 1.09	0.157, 0.553, 1.05	0.116, 0.339, 1.08
No. of parameters	845	960	612	936
No. of restraints	3015	990	881	1413
$\Delta\rho_{max}$, $\Delta\rho_{min}$ (e Å^{-3})	0.27, -0.22	0.23, -0.25	0.39, -0.44	0.42, −0.31
Absolute structure parameter	-0.008 (15)	Twinning involves inversion, so Flack parameter cannot be determined	-	-

Table S2. Weak noncovalent π-π and C-H···π interactions in crystals of C2- and C8-BFMPT at 200K. Cg is the aromatic ring center; D_{pln} is the nearest distance between H-atom or aromatic ring center and aromatic ring plane; α- interplane angle for interacting cycles; D and A are donor and acceptor of hydrogen bond, respectively. Cycle numbers for C2-BFMPT and C8-BFMPT-II are indicated according to Figure 4 and 5 (main text), respectively.

Compound	Interaction	Cg···Cg/H···Cg/ H···A (Å)	D_{pln} / D···A (Å)	C-H···Cg/α/ D- H···A (°)
C2-BFMPT	π7···π6	3.998(6)	3.312(4)	20.7(5)
	$C14^{(Cg\ 5B)}$-H···$\pi1^{(A)}$	2.83	2.82	146
	$C13^{(Cg\ 5A)}$-H···π4	2.91	2.81	123
	$C25'^{(A)}$-H···$\pi8^{(B)}$	2.86	2.76	138
	$C26'^{(A)}$-H···$\pi7^{(B)}$	2.73	2.69	141
	$C4'^{(A)}$-H···$\pi9^{(B)}$	2.68	2.62	169
	C15'-H···π7	2.77	2.73	154
	C25'-H···π4	2.68	2.61	140
	C13'-H···π2	2.64	2.64	146
C8-BFMPT Form II	C25'-H···π7	3.01	2.97	116
	C28-h28b···π9	2.81	2.79	149
	C2A-H2AA···π7	3.04	2.95	156

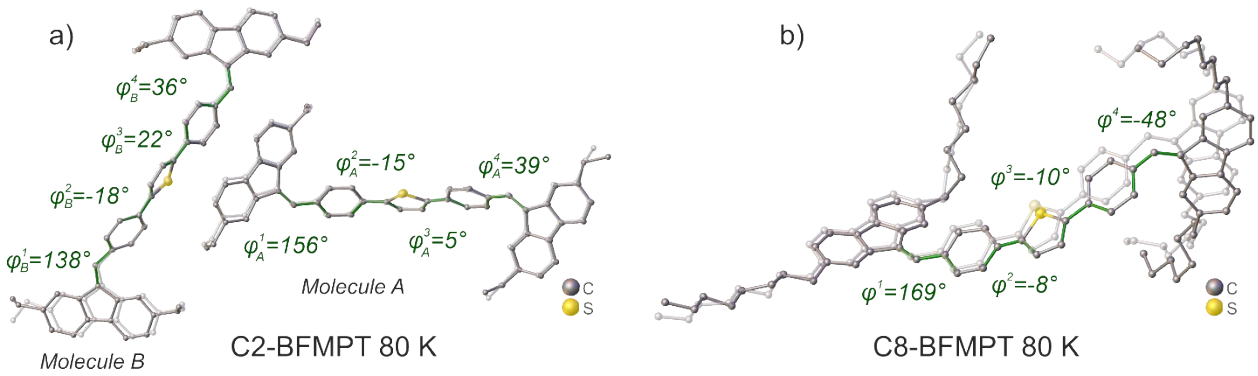

Figure S25. Molecular structures of C2- and C8-BFMPT at 80K with disordered groups (translucent) drawn with fixed atomic radii for clarity. The torsional angles are similar and the difference is no more than 10° as compared to that at 200K.

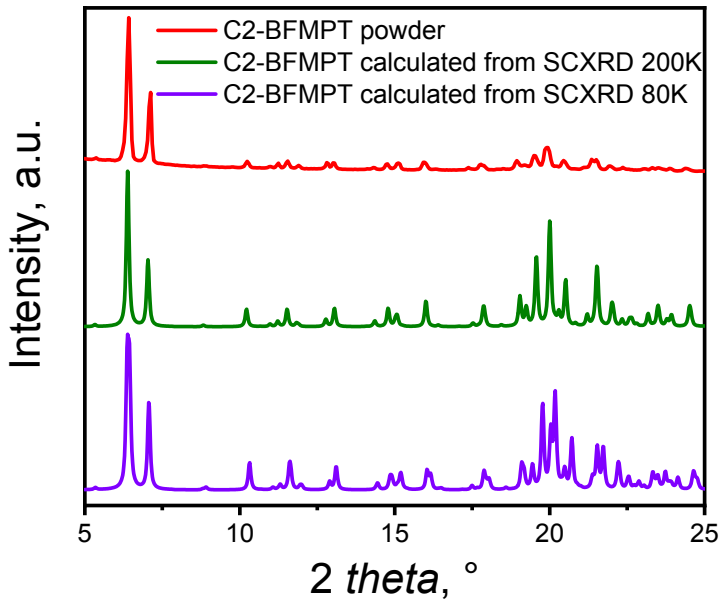

Figure S26. The powder X-ray diffraction powder patterns of C2-BFMPT at ambient temperature (red) and calculated from single-crystal X-ray data at 200 K (olive) and 80 K (violet). The slight shifts of the calculated patterns with respect to the measured ones are accounted for by the temperature differences.

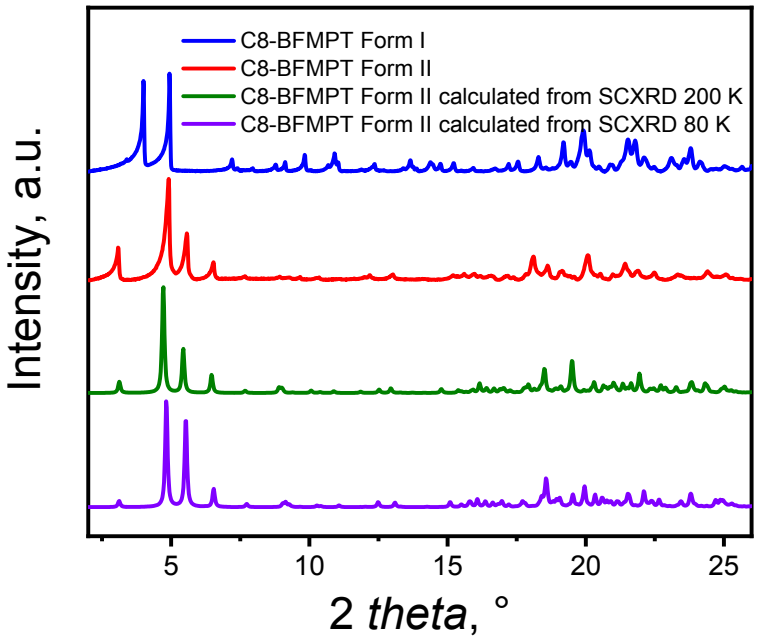

Figure S27. The powder X-ray diffraction patterns of C8-BFMPT: form I (blue), form II (red) at ambient temperature and the theoretical patterns of form II calculated from single-crystal X-ray data at 200 K (olive) and 80 K (violet). The slight shifts of the calculated patterns with respect to the measured ones are accounted for by the temperature differences.